

Extraction, purification, and reuse of dyes from coloured polyester textiles

Received: 2 November 2024

Accepted: 16 October 2025

Published online: 24 November 2025

 Check for updates

Minjung Lee  ^{1,2}, Yuanzhe Liang  ^{1,2,8}, Amy A. Cuthbertson  ^{1,2,9}, Samah Y. Mohamed  ³, Allen Puente-Urbina  ^{1,10}, William E. Michener ^{1,2}, Joel Miscall  ^{1,2}, Clarissa Lincoln ^{1,2}, Ciaran W. Lahive  ^{1,2,11}, Jason S. DesVeaux  ^{2,4}, Eli J. Fastow ⁵, Karen I. Winey  ^{5,6}, Hoon Choi  ^{1,2}, Brandon C. Knott  ^{1,2}, Natalie Banakis ⁷, Robert D. Allen  ^{1,2}, Gregg T. Beckham  ^{1,2}  & Katrina M. Knauer  ^{1,2} 

The removal of dyes from coloured textile waste represents a sustainable approach to textile recycling, enabling the recovery of valuable chemical, and material resources that would otherwise be discarded. Up to 40% of the greenhouse gas emissions from textiles originate from dye production, making efficient recycling of dyes a major opportunity for curbing emissions and minimizing waste in both textile manufacturing and recycling. Here we demonstrate a process for the extraction, purification, and reuse of mixed dyes from polyester textiles using bio-based, non-hazardous solvents selected on the basis of computational predictions for polyester and dye solubilities. Extracted dyes are purified to individual compounds using counter-current chromatography and analysed via liquid chromatography–mass spectrometry. Post-extraction characterization of the extracted dyes and polymer substrate confirms dye colour retention and polyester fabric property preservation. Dye recycling is demonstrated by redyeing colour-free fabrics with the recovered dyes. We further show a potential process configuration for dye removal using a flow-through reactor packed with a textile substrate. The proposed dye removal process produces reusable, recyclable dyes, and dye-free fabrics, thus facilitating textile recycling.

Textile manufacturing produces ~1.2 billion tons of greenhouse gas emissions annually, accounting for ~6–7% of the planet's total carbon budget^{1,2}. With textile consumption projected to reach 102 million tons with a concomitant greenhouse gas emissions increase of 30% by 2030, urgent action to reduce global warming is needed^{1,2}. One strategy to mitigate emissions and reduce waste from textile manufacturing is textile-to-textile recycling. Currently, mechanical recycling is the primary method for fibre recycling, involving the removal of ‘disruptors’

(for example, buttons, zippers, cuffs, and straps), garment washing and shredding, and melt extrusion into pellets for recycled fibre production. However, mechanical fibre recycling is challenged by the presence of dyes, which cause contamination, discoloration, and degradation in recycled fibres³. This is especially the case for poly(ethylene terephthalate) (PET) fibres, which account for 54% of global fibre production^{4,5}. Dyes can also be problematic in emerging chemical recycling methods that deconstruct PET fibres to monomers^{6,7}. Taken together, the

¹Renewable Resources and Enabling Sciences Center, National Renewable Energy Laboratory, Golden, CO, USA. ²Bio-Optimized Technologies to keep Thermoplastics out of Landfills and the Environment (BOTTLE) Consortium, Golden, CO, USA. ³Center for Integrated Mobility Sciences, National Renewable Energy Laboratory, Golden, CO, USA. ⁴Catalytic Carbon Transformation and Scale-Up Center, National Renewable Energy Laboratory, Golden, CO, USA. ⁵Department of Materials Science and Engineering, University of Pennsylvania, Philadelphia, PA, USA. ⁶Department of Chemical and Biomolecular Engineering, University of Pennsylvania, Philadelphia, PA, USA. ⁷Patagonia, Inc., Ventura, CA, USA. ⁸Present address: School of Chemical, Biological, and Environmental Engineering, Oregon State University, Oregon, OR, USA. ⁹Present address: Agilent Technologies, Wilmington, DE, USA. ¹⁰Present address: School of Chemistry, Costa Rica Institute of Technology, Cartago, Costa Rica. ¹¹Present address: Materials Engineering Department, University of Manchester, Manchester, UK.  e-mail: gregg.beckham@nrel.gov; katrina.knauer@nrel.gov

development of an efficient method to extract dyes from waste fibres, which ideally could recover and purify dyes for reuse, holds promise for both established and emerging textile recycling platforms.

Multiple solvent-based treatments have been proposed for dye removal from PET fabrics, including the use of organic solvents^{3,8–14} and supercritical carbon dioxide¹⁵. To date, effective solvent-based dye extraction has been shown with conventional organic solvents including xylene^{8,9}, dimethylformamide⁹, dimethyl sulfoxide^{9,11,16}, 1,3-dimethyl-2-imidazolidinone¹⁷, alkylene glycols (for example, ethylene glycol)^{8,9,12}, and ether-alcohol solvents such as diethylene glycol monoethyl ether¹⁰. Bio-based solvents present promising alternatives due to their potentially lower toxicity and reduced life-cycle impacts on the extraction process¹⁸. Recent studies have begun exploring dye removal from fibres using bio-based solvents^{3,11,12}, demonstrating their effectiveness in dye extraction. Subsequent dye recovery, separations, and reuse, however, are critical factors that remain to be investigated.

When the colour and chemical structure of dyes are maintained during an extraction process, recovered dyes can be separated from the extraction solvent and reused in textile dyeing. In particular, membrane-based separation is a promising technique for dye isolation from dye/solvent mixtures due to mechanical simplicity, the ability to operate continuously, low energy requirements and high product recovery^{19,20}. Extracted dyes are typically mixtures of multiple dye compounds combined to achieve a specific colour. These mixtures can be further separated into individual dye molecules via chromatography techniques. Counter-current chromatography (CCC)^{21,22}, a hydrodynamic type of liquid–liquid chromatography that uses a biphasic solvent system for both liquid stationary and mobile phases, has been used to produce highly pure molecules from complex systems. CCC could also be an effective tool for recovering isolated dye compounds from mixtures^{23,24}.

In this study, we develop a solvent-based dye extraction, recovery, and reuse process for post-consumer PET-rich fabrics. We first screen 20 solvents that have the potential to be sourced from bio-based feedstocks and exhibit low human health impacts via conductor-like screening model for realistic solvents (COSMO-RS) calculations for PET and dye solubilities, followed by experimental evaluation. Four solvents are selected as promising candidates for dye removal: acetic acid, 4-ethylguaiacol (4-EG), 4-propylguaiacol (4-PG), and 4-propylphenol (4-PP). The extracted dyes are separated into individual dye compounds using CCC, and the separated dye fractions are characterized via liquid chromatography–mass spectrometry (LC–MS). To demonstrate the recyclability of the recovered dye mixtures, we successfully redye natural (that is, undyed and without chemical finishings) PET fabrics. Lastly, we demonstrate a potential process configuration for dye removal from PET textiles using a packed-bed reactor with solvent flow-through.

Results

Solubility prediction for disperse dyes and PET

An ideal solvent for dye extraction will selectively dissolve the dyes, facilitating the diffusion of the dyes out of the PET matrix and into the extraction solvent²⁵. The solubility of PET and commonly used disperse dyes (Orange 30, Red 167.1, and Blue 79.1) was estimated through molecular dynamics (MD) simulations and COSMO-RS calculations^{26–28} (Fig. 1a and Supplementary Fig. 1). Density functional theory calculations were first performed using Gaussian 16 (ref. 29) to generate the COSMO polarization charge-density profiles for the 20 bio-based solvents, two control solvents (diethylene glycol monoethyl ether and water), a PET trimer, and the three dyes. For PET, multiple trimer configurations were selected from a 10-ns MD trajectory, and multiple low-energy conformers for the dyes and solvents were also selected (as described in the Methods). The generated charge-density profiles were then used in COSMO-RS calculations, as implemented in COSMOtherm³⁰, to predict the solubilities of PET and dyes in each solvent

(listed in Supplementary Table 1) at 25 °C and 100 °C. The results are shown for PET and Orange 30 in Fig. 1b,c and Supplementary Table 2.

Orange 30 dye was predicted to exhibit a distinctly lower solubility at both modelled temperatures in four solvents: (R)-(+)-limonene (limonene), ethylene glycol (EG), poly(ethylene glycol) with a molar mass of 200 Da (PEG 200) and PEG 400. For PET, 4-PP, 4-isopropylphenol (4-IPP), and thymol exhibited relatively higher solubility (~0.28 g g⁻¹) than the other tested solvents at 25 °C, and the solubility of most solvents was predicted to be higher at 100 °C than at 25 °C. The PET solubility is 2.7 to 47 times lower than the dye solubility at 25 °C and 1.3 to 4.7 times lower than the dye solubility at 100 °C. This feature is particularly desirable for a dye extraction process, where dissolution of the dyes while maintaining the PET fibres intact could facilitate downstream recycling of the fibres. The complete dataset for Orange 30, Red 167.1, Blue 79.1, and PET is provided in Supplementary Fig. 2 and Supplementary Table 2. Similar trends were observed across the dyes at 100 °C. Furthermore, the partition coefficient ($\log P$) of the dyes was predicted by COSMO-RS calculations to evaluate the relative affinity of dyes for PET fabric or the solvents (Supplementary Fig. 3 and Supplementary Table 3). The four solvents (limonene, EG, PEG 200, and PEG 400) showed negative $\log P$ values at both 25 °C and 100 °C, suggesting a stronger affinity for the PET fabric than the solvents.

To verify the solubility and the $\log P$ predictions above, a dye extraction experiment was conducted on PET fabrics dyed with Orange 30 in different solvents (Fig. 1d,e). The Orange-30-dyed fabric was prepared via exhaust dyeing²⁵ and subjected to a dye extraction process. Here we chose a solvent treatment method based on previous studies^{3,9,11} using solvents at temperatures above the glass transition temperature of PET (~70 °C)³¹, to promote the release of the dyes. Among the solvent-treated fabrics (Fig. 1d), some exhibited a relatively white colour, indicating effective dye extraction, while others retained an orange colour, indicating ineffective dye extraction. The colour measurement and the mass loss of the fabrics after solvent treatment are detailed in Supplementary Tables 4 and 5. Among the eight solvents with ineffective dye extraction listed in Supplementary Table 5, limonene, EG, PEG 200, and PEG 400 were predicted to be inefficient by COSMO-RS, as they exhibit lower solubilities than the other solvents in Fig. 1b,c. These four solvents were also predicted to partition into PET with negative $\log P$ values.

Additionally, the solutions obtained after the solvent treatment (Fig. 1e) provide insights into the impact that the solvents exhibit on dye integrity. Orange-coloured solutions suggest that the chemical integrity of the dye was retained, while the colourless γ-valerolactone (GVL) solution suggests that a chemical transformation occurred. GVL is a known oxidizing agent³², and it is possible that dye decomposition occurred at elevated temperatures in GVL. The extracted Orange 30 dye in acetic acid exhibited UV–Vis spectra comparable to those of the original dye, indicating an intact chemical structure (Supplementary Fig. 4).

Combining the experimental results with the COSMO-RS data identified 12 potential solvents for effective dye extraction with colour retention of the extracted dyes from PET fabrics: acetic acid, 4-EG, 4-PG, 4-PP, benzyl alcohol, cyrene, ε-caprolactone, guaiacol, eugenol, isoeugenol, 4-IPP, and thymol.

Dye extraction from coloured PET fabrics

To understand the practicality of this approach on realistic substrates, we subsequently evaluated the dye extraction process using commercial post-industrial waste fabrics, encompassing multiple unknown dye chemistries and a range of garment types (namely, jersey, woven, and fleece fabrics). This selection served as a representative sample of the diversity found in PET clothing waste. Specifically, we used eight PET-rich garments (verified via infrared; Supplementary Figs. 5a and 27a) with varied colours and textures supplied by Patagonia, Inc.: red-jersey, blue-jersey, green-jersey, orange-woven, green-woven, black-woven, black-fleece, and grey-fleece. Four solvents (acetic acid,

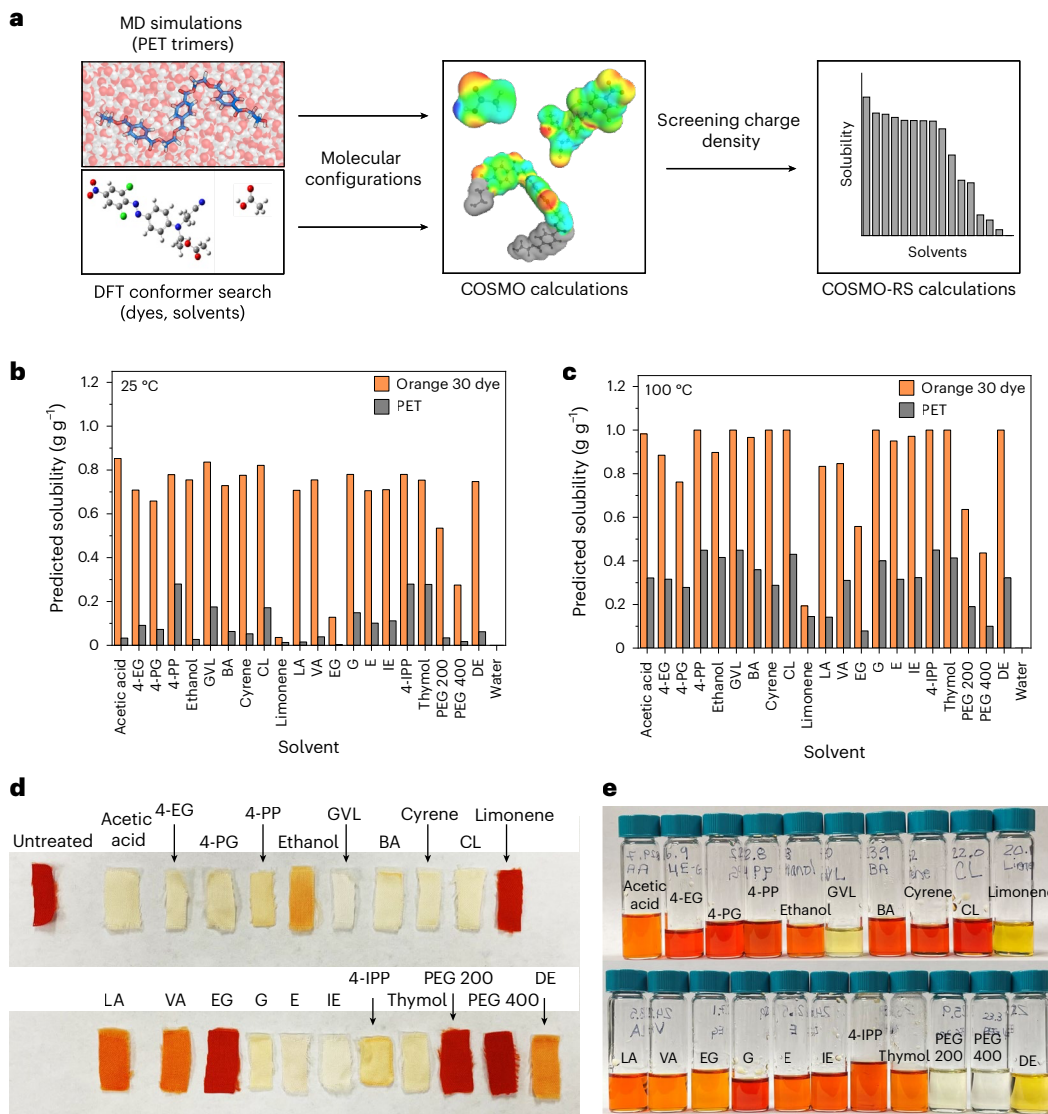


Fig. 1 | Solubility predictions of PET and dyes from COSMO-RS calculations. **a**, Workflow to obtain solubility prediction. **b,c**, Predicted solubility of PET and Orange 30 dye at 25 °C and 100 °C in 22 solvents: acetic acid, 4-EG, 4-PG, 4-PP, ethanol, GVL, benzyl alcohol (BA), cyrene, ϵ -caprolactone (CL), limonene, levulinic acid (LA), valeric acid (VA), EG, guaiacol (G), eugenol (E), isoeugenol (IE).

4-IPP, thymol, PEG 200, PEG 400, diethylene glycol monoethyl ether (DE), and water. **d**, PET fabrics with Orange 30 dye including an untreated control substrate and samples after dye extraction at 100 °C for 16 h in different solvents. **e**, Dye-extracted solutions from the PET fabrics shown in **d**.

4-EG, 4-PG, and 4PP) were down-selected for further experiments, on the basis of the COSMO-RS predictions, initial solvent screenings (Supplementary Figs. 7–10), potential to be sourced from bio-based feedstocks, and predicted low human health toxicity (Supplementary Table 1). These selected solvents were evaluated for their ability to remove unknown dyes from the eight fabrics mentioned above (Supplementary Figs. 5 and 6). The degree of dye removal was assessed visually (Fig. 2a and Supplementary Figs. 5 and 6) and through spectroscopic colour measurements (Supplementary Fig. 11 and Supplementary Table 6). Furthermore, optical micrographs of the solvent-treated fabrics confirmed no significant changes of the fabrics themselves during the dye extraction process (Supplementary Fig. 12).

As depicted in Fig. 2a, the solvent-treated fabrics exhibited a noticeably whiter appearance than the untreated fabrics, indicating significant dye extraction. However, the red dyes proved to be more recalcitrant, still displaying a light pink hue under regular testing conditions, presumably due to stronger interactions between the PET fibres and the red dye. To enhance the dye extraction from red fabrics, we increased both the temperature (up to 150 °C) and the

exposure time (up to 72 h) (Fig. 2c,d and Supplementary Fig. 13). We observed that dye extraction improved at higher temperatures and longer times, as evidenced by the lighter colour of the treated fabrics. However, slight yellowing of the fabric was observed, indicative of PET degradation, which was confirmed by the reduced molar mass (Supplementary Fig. 14 and Supplementary Table 7). The colour change in the red-jersey dye upon extraction suggests potential degradation of the dye at higher temperatures (Fig. 2d and Supplementary Fig. 13), rendering it unsuitable for reuse, which could be mitigated through changing the process configuration (*vide infra*). We also tested other types of fabric for dye extraction, including denim (cotton), poly-cotton, nylons, and a nylon/spandex blend (Fig. 2e, Supplementary Figs. 15 and 16 and Supplementary Table 8).

Another indicator of effective dye extraction is the mass loss of the treated PET fabric, which could include dyes, microfibres, and other additives (Fig. 2b). The mass loss observed for acetic-acid-, 4-EG-, and 4-PG-treated fabrics is comparable. However, the mass loss for 4-PP-treated fabrics is more than twice the values of the other solvents. We attribute this discrepancy to the higher solubility of PET

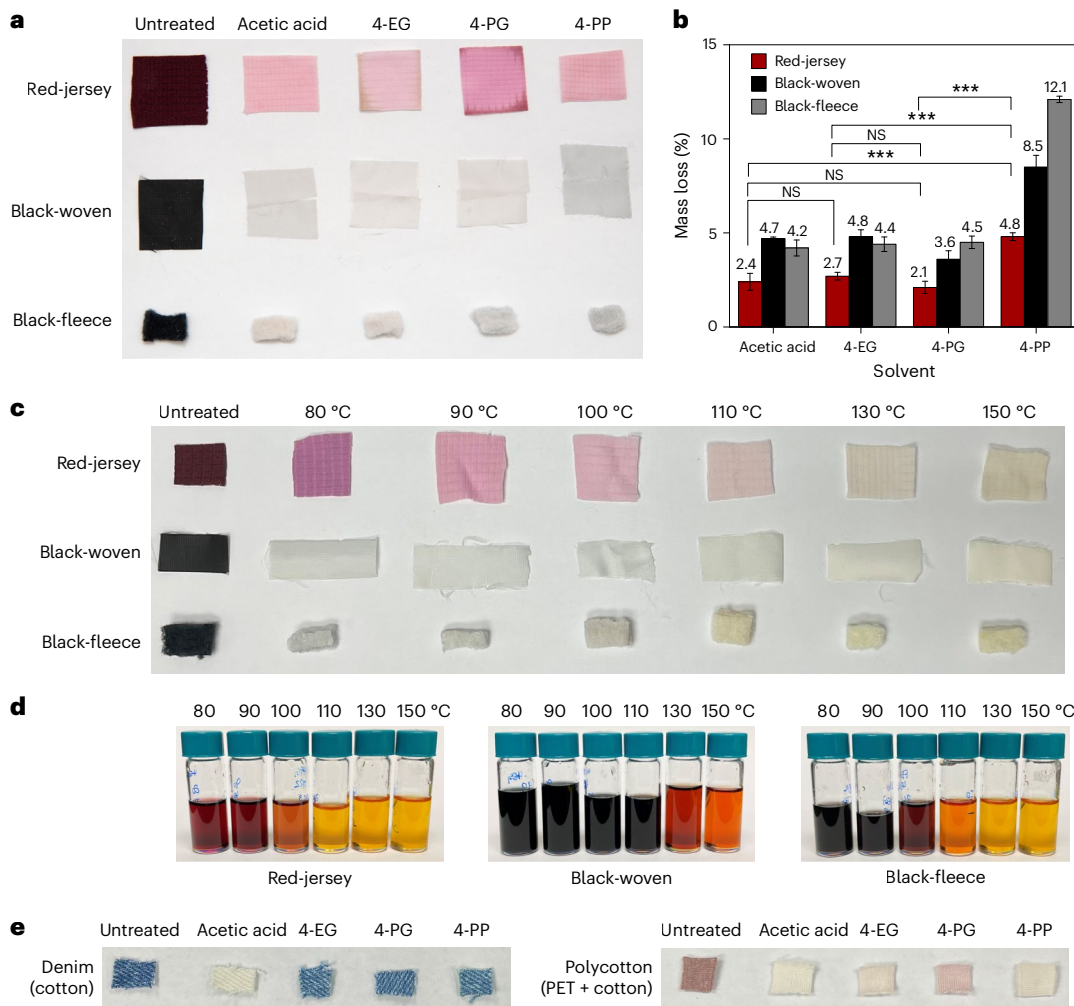


Fig. 2 | Dye-extracted PET fabrics and solutions. **a**, Representative PET fabrics supplied by Patagonia, Inc. (red-jersey, black-woven, and black-fleece) before and after solvent treatment at 100 °C for 16 h in the four top-performing solvents: acetic acid, 4-EG, 4-PG, and 4-PP. **b**, Mass loss values for each fabric after solvent treatment. Each bar and its error bar represent the mean and standard deviation of triplicate measurements, respectively. Student's *t*-test (two-sided) shows that the differences between acetic acid and 4-EG, acetic acid and 4-PG, and 4-EG and 4-PG are not significant (NS), while the differences between acetic acid and 4-PP ($P = 0.0007$ for red-jersey, $P = 0.0004$ for black-woven, $P < 0.0001$ for black-fleece), 4-EG and 4-PP ($P = 0.0002$ for red-jersey, $P = 0.0009$ for

black-woven, $P < 0.0001$ for black-fleece), and 4-PG and 4-PP ($P = 0.0002$ for red-jersey, $P = 0.0003$ for black-woven, $P < 0.0001$ for black-fleece) are very highly significant (** $P < 0.001$) for all three fabrics. Note that the mass loss includes both the extracted dyes and PET fibre loss. The PET fibre loss in 4-PP is greater than that in the other three solvents. **c**, PET fabrics before and after solvent treatment in 4-EG as a function of temperature from 80 to 150 °C.

d, Dye-extracted solutions from the PET fabrics shown in **c**. **e**, Denim (cotton) and polycotton (PET + cotton) before and after solvent treatment. Note that the dye extraction experiment above was performed with 1 wt% of fabric in each solvent at the given temperature for 16 h.

in 4-PP (as predicted by COSMO-RS; Fig. 1b,c), which may allow for higher solubilization of PET oligomers and microfibres during the extraction process. We also measured the mass loss of the treated PET under different conditions such as temperature, concentration, and time (Supplementary Fig. 17). The increased temperature varying from 80 to 150 °C resulted in a slight increase in mass loss. The fabric concentration varying from 1 to 12 wt% changed the mass loss in the range of 2.3–2.9 wt% for red-jersey and 3.8–4.7 wt% for black-woven. However, black-fleece showed a sudden increase in mass loss (from 3.2 to 8.1 wt%) when the fabric concentration increased from 5 wt% to 8 wt%. This is attributed to increased polymer loss during dye extraction, as confirmed by the observation that fibre fragments detached and dispersed into the solution.

Properties of recovered PET fabrics after dye extraction

To evaluate the impact of the dye extraction process on the PET structure, the physicochemical and thermal properties of the PET fabrics were investigated before and after extraction, via gel permeation

chromatography (GPC), differential scanning calorimetry (DSC), thermogravimetric analysis (TGA), and X-ray scattering. Comparison of GPC chromatograms before and after solvent treatment revealed that the molar mass of the PET fabrics is virtually unaffected by the solvent treatment (Fig. 3a–c and Supplementary Table 9). Interestingly, the GPC traces of untreated fabrics exhibited not only the polymer peak at ~33 min but also additional small-molecule peaks between 40 and 45 min. These peaks are attributed to the dye compounds in the untreated PET matrix, which were absent in the traces of the treated fabrics, indicating successful removal of dyes and potentially other additives without chemical degradation of the PET. The thermal properties and crystallinity of the treated PET fabrics did not show significant changes during the dye extraction process (Fig. 3d–i). Furthermore, X-ray scattering analysis was conducted to investigate the crystal structure of the PET fabrics. The results confirmed that the local crystal structure (Supplementary Tables 10 and 11) and semicrystalline microstructure (Supplementary Tables 12 and 13) of the treated PET were unaltered by the dye extraction process for both the dry (that is, after

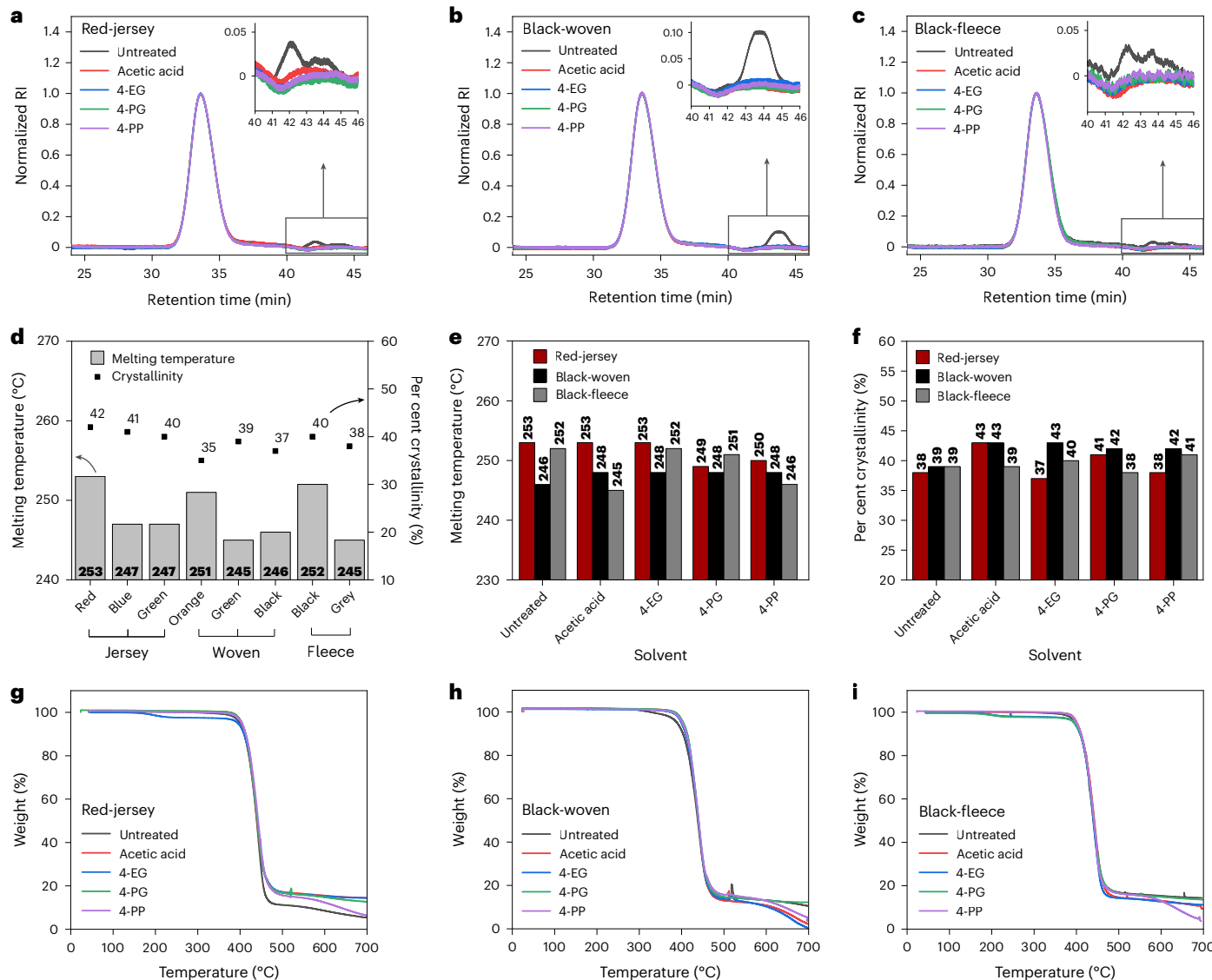


Fig. 3 | Recovered PET properties after dye extraction. **a–c**, GPC traces of PET fabrics for red-jersey (**a**), black-woven (**b**), and black-fleece (**c**) before and after solvent treatment at 100 °C for 16 h in acetic acid, 4-EG, 4-PG, and 4-PP. RI, refractive index. **d**, Thermal properties of the initial eight fabric materials; red-jersey, blue-jersey, green-jersey, orange-woven, green-woven, black-woven, black-fleece, and grey-fleece. **e,f**, Melting temperatures (**e**) and per cent

crystallinity (**f**) of PET fabrics for red-jersey, black-woven, and black-fleece before and after solvent treatment at 100 °C for 16 h in acetic acid, 4-EG, 4-PG and 4-PP. **g–i**, Thermal degradation behaviours of PET fabrics for red-jersey (**g**), black-woven (**h**), and black-fleece (**i**) before and after solvent treatment at 100 °C for 16 h in acetic acid, 4-EG, 4-PG, and 4-PP. DSC (**d–f**) and TGA (**g–i**) were used for these measurements. The DSC data in **d** are separate from those in **e** and **f**.

solvent removal) and wet (that is, in the presence of solvent) states. Taken together, these findings show that the PET structure remains intact after dye extraction. As we envision the mechanical recycling of dye-extracted PET fabrics (Supplementary Fig. 18), the melt extrusion of dye-extracted PET fibres was performed to compare the properties of the ‘recycled product’ with those of post-consumer PET bottle flakes. PET fabrics, and bottle flakes demonstrated similar changes in colour and molecular weight during mechanical recycling, indicating that dye-free fibres can be recycled alongside bottle flakes (Supplementary Fig. 19 and Supplementary Tables 14 and 15).

Fractionation and characterization of extracted dye mixture

To separate and purify the extracted dye mixtures for potential reuse, we first obtained the dried dye mixture through solvent evaporation. Using the dried dye mixtures, we applied CCC, a liquid–liquid chromatography method that leverages differences in partition coefficients in a biphasic solvent system to separate multiple

components simultaneously (Fig. 4a). Traditionally, the Arizona system (heptane, ethyl acetate, methanol, and water) is used as the biphasic solvent in CCC²¹, but here we replaced ethyl acetate with cyclopentyl methyl ether, which is a more environmentally friendly solvent³³. Among the tested solvent compositions, a 3:1:3:1 volume ratio of heptane, cyclopentyl methyl ether, methanol, and water (HCMWat) was optimal for separating the four dye mixtures extracted from the red-jersey, blue-jersey, green-jersey, and black-woven fabrics.

The CCC fractions collected from the red-jersey dye mixture are shown in Fig. 4b. Successful separation of multiple dyes is evident from the diverse colours observed in the CCC fractions. Each dye fraction was characterized via LC–MS to identify its molar mass in the visible wavelength regime (Fig. 4c). Given that the lower phase (aqueous/polar phase) was used as the mobile phase, polar compounds eluted earlier than non-polar ones. Of the 14 CCC fractions collected from the red-jersey dye mixture (Supplementary Figs. 20 and 21), only 5 exhibited distinct colours as observed in the LC–MS

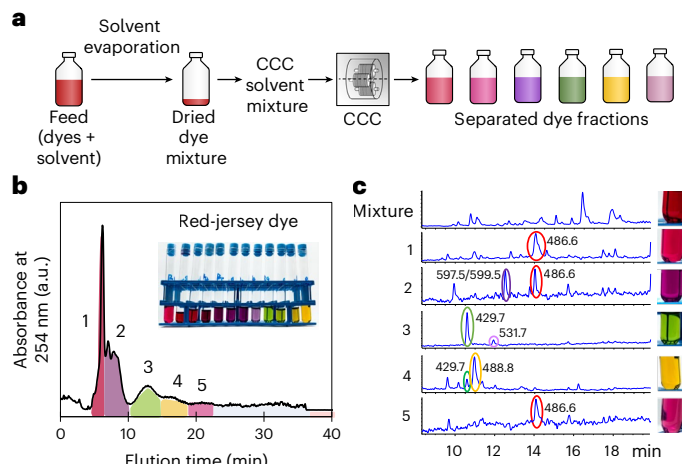


Fig. 4 | Dye separation using CCC. **a**, Workflow to obtain separated dye fractions using CCC. **b**, CCC chromatogram of the red-jersey dye mixture using an HCMWat (3:1:3:1) solvent system in the reverse phase (lower mobile phase). The inset photo shows the separated dye fractions from the red-jersey dye mixture using CCC. **c**, LC-MS data of the red-jersey dye mixture and the separated dye fractions as CCC effluents, as labelled in the CCC chromatogram in **b**. The $[M + H]$ values provided were compounds with strong responses in the wavelength of the visible range.

chromatograms (Fig. 4c). The extracted dyes exhibited molar mass values ranging from 429.7 to 599.5 Da (Fig. 4c). Some MS peaks (for example, 486.6 and 429.7 Da) were observed between two effluent fractions due to peak overlap with similar retention times in CCC, suggesting the need for further optimization to fully separate dyes from each other. Interestingly, fractions 1 and 5 both exhibited a pink colour and the same molar mass (486.6 Da), despite the expectation of more non-polar groups in fraction 5. The other dye mixtures (blue-jersey, green-jersey, and black-woven dyes) were also successfully separated using CCC with the HCMWat solvent system (Supplementary Figs. 20–22), highlighting the versatility of CCC for multiple, unknown dye mixtures.

Recycling of extracted dyes

To demonstrate dye reuse, we redyed the dye-free PET fabrics with the extracted dyes by applying the exhaust dyeing method. The closed-loop process included (1) extracting dyes from the commercially-derived, coloured PET fabrics using acetic acid; (2) removing the extracted dye from acetic acid via organic solvent nanofiltration (OSN) to recover a concentrated dye mixture (Supplementary Fig. 23); and (3) redyeing the same fabrics using the concentrated dyes via exhaust dyeing. As seen in Fig. 5, while there is a slight difference in the colour intensity between the untreated fabrics (Fig. 5a) and the redyed fabrics (Fig. 5c and Supplementary Table 16) due to the partial loss of dye contents during dye recovery processes and to differences between laboratory-based dyeing and industrial-scale processes, the original hues of the dyes were maintained.

Dye extraction demonstration in a flow-through reactor

Finally, to demonstrate dye extraction in a flow-based process, we used an 80-ml tubular reactor with acetic acid as the extraction solvent (Fig. 6a). Red-jersey fabric pieces ($5 \times 5 \text{ mm}^2$) were packed in the reactor, with temperature measured by three thermocouples along the reactor length. Dye-containing solutions were collected as samples over time after acetic acid was passed through the reactor, and the dye-extracted fabric was collected after the experiment (Fig. 6b). The red-jersey fabric was selected for this experiment as it was found to be the most challenging dye to fully extract, and we posited that a flow reactor, involving a continuous flow of pure acetic acid at a high temperature through the fabric, would enhance the dye extraction.

To achieve effective dye removal and preservation from recalcitrant red-jersey fabric, three separate extraction experiments were conducted under three different temperature settings: (1) constant temperature at 100°C , (2) initial temperature at 100°C followed by holding at 150°C , and (3) initial temperature at 100°C followed by holding at 180°C . The second heating stages (150°C or 180°C) were initiated when the red-jersey dye colour began to fade (Fig. 6b). We hypothesized that extraction at 100°C would ensure dye preservation in the solution, while subsequent extraction at 150°C or 180°C would enhance dye removal from the red-jersey fabric. The reactor outlet temperature for each experiment was used to control the desired temperature (100°C , 150°C , or 180°C), and it was reached by heating the transfer line and the reactor. Temperature profiles from the three thermocouples placed in the reactor for each experiment are shown in Supplementary Fig. 24. The preheating step resulted in sample 1 exhibiting a negligible dye concentration. In contrast, samples 2 and 3 showed the highest dye concentration (approximately 0.25–0.3 wt%) within the initial 30–60 minutes, followed by a rapid decline in the subsequent 60–120 minutes (samples 3–5) (Fig. 6b,c and Supplementary Fig. 25).

The flow-through reactor allowed for higher loading of the fabric substrate (~5 g; fabric concentration to the total solvent amount used, 1.9–2.4 wt%) and lower operating times (~5 h) than the batch system (~50 mg, 1 wt%, 16 h). Moreover, the extent of dye extraction was enhanced using the flow-through reactor compared with the batch experiments using the red-jersey fabric (Supplementary Tables 6 and 17). Dye extraction was also enhanced with increasing operating temperatures. However, the flow reactor experiments showed more pronounced effects on the PET structure. The molar mass of the PET fabric decreased by 12%, 16%, and 28% for the 100°C , 150°C , and 180°C samples, respectively (Fig. 6d and Supplementary Table 18). This reduction in molar mass suggests degradation of the PET backbone during extraction. Nonetheless, similar to the batch experiments, the removal of small molecules was confirmed by the absence of peaks around 28–32 min in GPC traces of the treated red-jersey fabrics (Fig. 6d). Reductions in melting point and the per cent crystallinity of the PET fabric were also observed by 1.6% and 25%, respectively, as shown for the 180°C samples (Fig. 6e), although the thermal degradation temperature remained unaffected (Supplementary Fig. 26).

Discussion

This study demonstrates the effective extraction of disperse dyes from PET-based textiles, resulting in a cleaner fibre feedstock for mechanical recycling and enabling textile-to-textile recycling. The recovered dyes can be separated from the extraction solvent through OSN and purified into individual dye molecules using CCC. While the results of this study are promising, several limitations and implications must be considered for further development. Although several solvents proved effective in dye extraction, those with low boiling points (but higher than the extraction operating temperature), low viscosity, and low toxicity are likely more ideal for process viability. Considering the



Fig. 5 | Overview of dye recycling. **a–c**, The PET fabrics in different stages: untreated (**a**), dye extracted (**b**), and redyed with the extracted dyes (**c**).

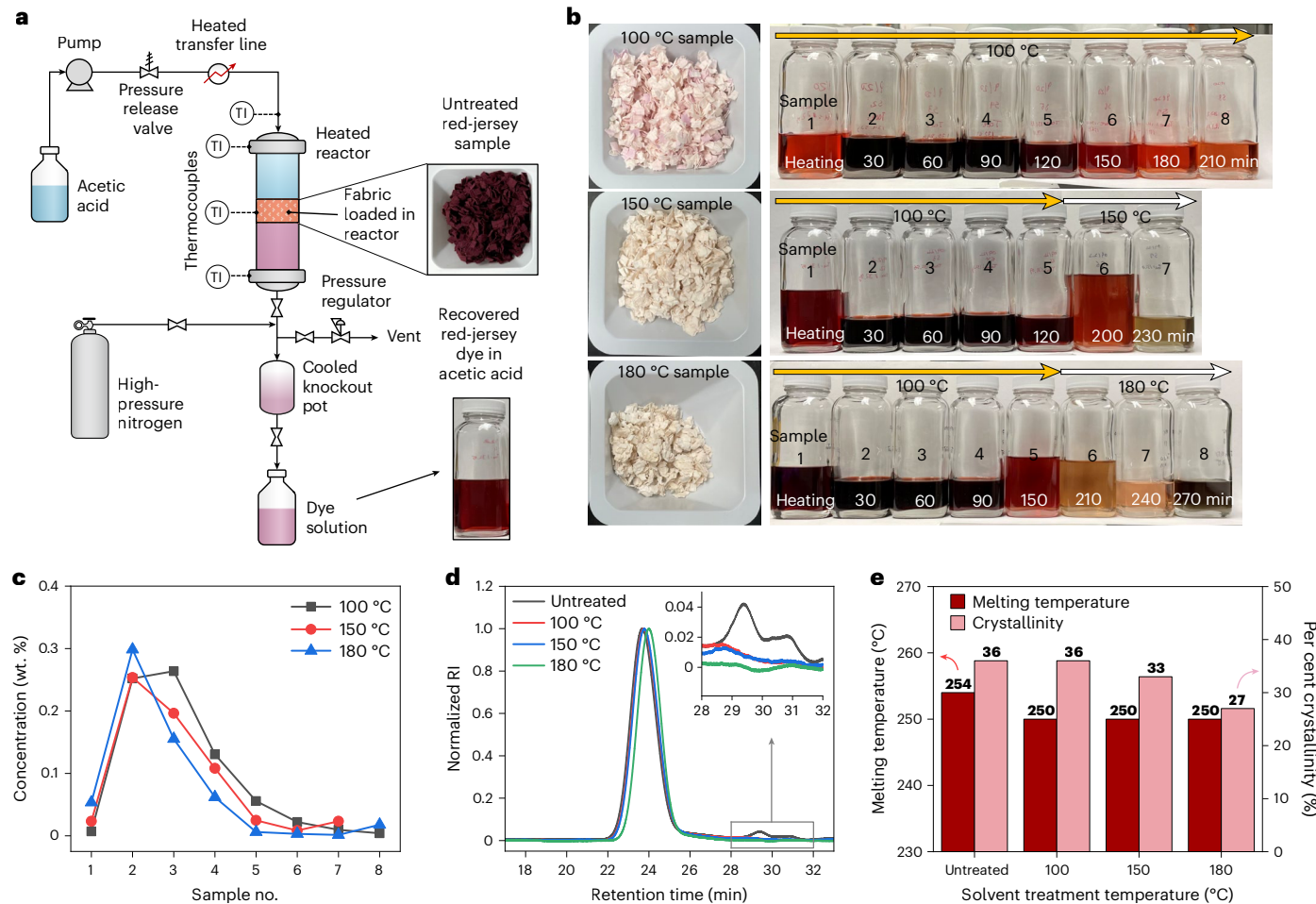


Fig. 6 | Dye extraction demonstration using a flow-through reactor. **a**, Scheme of the flow-through reactor. **b**, The red-jersey fabrics and dye solutions after solvent treatment at different temperatures in acetic acid. **c**, Concentration of the red-jersey dye in each dye solution shown in **b**. The concentration value was obtained by measuring the UV–Vis absorption of each solution at the maximum

intensity (505 nm) and calculating the red-jersey dye concentrations on the basis of the Beer–Lambert law. **d**, GPC traces of the red-jersey fabric before and after solvent treatment at different temperatures in acetic acid. **e**, Melting temperature and per cent crystallinity of the red-jersey fabric before and after solvent treatment at different temperatures in acetic acid.

feasibility of scaling the proposed process, acetic acid appears to be the most optimal extraction solvent due to its availability in high volumes, low cost, widespread industrial use, ease of safe handling and potential to be sourced from bio-based resources.

To scale the proposed process with acetic acid for textile recycling, efficient solvent recycling is crucial to maintain favourable economics and minimal environmental impacts. In this work, OSN was used to separate the dyes from the extraction solvent, demonstrating that the solvents can be recovered and reused in the process (Supplementary Fig. 23). However, OSN may not yet be feasible on a large scale due to low flux and high membrane costs. When acetic acid is used as the extraction solvent, flash or vacuum distillation could be a promising alternative for solvent recovery at scale. Given that the process operates at temperatures between 100 and 150 °C, which is within the boiling point range of acetic acid (118 °C), flash distillation^{34,35} could recover a significant portion of the solvent for reuse.

Extracted dyes can be further separated into individual formulation components via CCC after separation from acetic acid. CCC-based separation approaches are in the early stages of development and have opportunities for improvement. As a chromatographic technique, batch CCC provides purified products that are diluted two to five times relative to their feed concentration, depending on retention in the column. The product dilution results in large solvent consumption and high energy duty for the subsequent solvent recovery. To overcome product dilution, the product concentration needs to be increased

while minimizing solvent consumption, which requires increasing the feed concentration, reducing the solute retention time, and ideally transitioning to a continuous CCC process. The nascent of CCC also makes it difficult to estimate the quantity and range of dyes that could be separated and used to replace new dyes. In the interim, an alternative, immediate reuse pathway is to repurpose these dye mixtures as black dyes, which is a common industrial practice. The global market volume for black dyestuffs (that is, mixed black dyes) in textile applications exceeds \$1 billion, underscoring the potential value and volume of this reuse strategy³⁶. Lastly, although this study demonstrated the use of CCC for dispersed dye separations, techno-economic analysis and life-cycle assessment of the full downstream process including product and solvent recovery will be required to evaluate the feasibility of using CCC in comparison to other separations, such as distillation alone or OSN/flash distillation. Understanding the economics and environmental impacts of the overall process can provide important criteria in the selection of a solvent and conditions for an industrially viable process.

In summary, we developed and demonstrated a conceptual process for the extraction, purification, and reuse of mixed dyes from polyester textiles. Integrating this technology into existing PET mechanical recycling systems has the potential to enable the additional recycling of up to 48 million tons of PET waste annually³⁷. While further techno-economic analysis and life-cycle assessment are needed to assess scalability, the low cost of acetic acid and the

simplicity of the extraction process suggest strong potential for industrial application.

Methods

MD simulations

Initial system set-up was performed in CHARMM v.44 (ref. 38), and subsequent minimization and dynamics were performed with NAMD v.2.13 (ref. 39). The CHARMM C36 force field^{40,41} was used for PET with topologies, and additional force-field parameters were generated via the CHARMM generalized force field (CGenFF) program v.2.5 (refs. 42,43) (Supplementary Tables 20 and 21). The TIP3P model was used for water^{44,45}. A PET trimer was created from the atomic coordinates reported by Daubeny et al.⁴⁶ with chain ends capped with EG motifs. The PET trimer was then solvated in a 50 Å × 50 Å × 50 Å box of TIP3P water molecules. Periodic boundary conditions were applied in all three dimensions. In NAMD, a conjugate gradient minimization was performed for 3,000 steps. The box volume and atomic positions were then equilibrated for 1 ns at constant pressure (1 atm) and temperature (300 K). A Langevin thermostat with a collision frequency of 1 ps⁻¹ was used to maintain the temperature at the target of each simulation. Pressure was maintained at 1 atm using a modified Nosé–Hoover method⁴⁷ in which Langevin dynamics was used to control fluctuations in the barostat^{48,49} with a damping time of 100 fs and a period of 200 fs. A non-bonded cut-off distance of 12 Å was used, with a switching distance of 10 Å and a non-bonded pair list distance of 16 Å. The long-range electrostatics were described via the particle mesh Ewald method⁵⁰ with a sixth-order β-spline and 1-Å grid spacing. The velocity Verlet time-stepping integration method was used, with the full non-bonded interactions, full electrostatics interactions, and atom reassignments evaluated on every time step. For all MD simulations, a time step of 2 fs was used. The SHAKE algorithm⁵¹ was used to keep bonds to hydrogen atoms fixed. A 10-ns NVT production run followed NPT equilibration. The molecular configuration was output every 10 ps, and the 20 PET conformations with the lowest internal potential energy were selected for subsequent optimization and COSMO surface charge calculations.

COSMO-RS

Geometry optimization and COSMO calculations to generate the COSMO files were performed for multiple conformers of PET, solvents, and dyes at the BVP86/TZVP/DGA1 level of theory as implemented in Gaussian 16 (ref. 29).

It has been demonstrated that more accurate solubility predictions are obtained when several conformers are considered in the calculations^{52,53}. Low-energy conformers of solvents and dyes were located using conformational analysis in Gaussian 16 (ref. 29) by rotating all hindered rotors, except C–CH₃ rotors, by 120°, generating 3ⁿ conformers. For each of the three reported dyes (Orange 30, Blue 79.1, and Red 167.1), the 20 distinct lowest-energy conformers were considered; for solvents, any distinguishable conformers within 1 kcal mol⁻¹ of the lowest-energy conformer were considered. For PET configurations, 20 conformers of a PET trimer in aqueous solution were selected from a single 10-ns MD trajectory as described above.

The COSMO files were then used in COSMOtherm³⁰ to determine the solubilities of PET and dyes in each solvent at 25 °C and 100 °C. BP_TZVP_22 parameterization was used for all the COSMO-RS calculations. For PET with 39% crystallinity, a melting temperature of 260 °C, as measured in this work, and enthalpy of fusion of 54.3 J g⁻¹ (refs. 54,55) were used. The solubility x_i of solute i was calculated as:

$$\log(x_i) = (\mu_i^{\text{pure}} - \mu_i^{\text{solvent}} - \Delta G_{\text{fus}}) / RT \ln(10) \quad (1)$$

μ_i^{pure} is the chemical potential of the pure solute i , and μ_i^{solvent} is the chemical potential of the solute i at infinite dilution in the solvent. ΔG_{fus} is the solute's Gibbs free energy of fusion. R is the gas constant, 8.314 J·K⁻¹mol⁻¹, T is the absolute temperature in Kelvin.

Partition coefficient predictions for disperse dyes between PET and solvents

COSMO-RS calculations were also used to determine the log P values of the commonly used disperse dyes (Orange 30, Red 167.1 and Blue 79.1) between PET (phase 1) and various solvents (phase 2). The log P values were computed using the equation:

$$\log(P_j^{(2,1)}) = (\mu_j^{(1)} - \mu_j^{(2)}) / RT \ln(10) + \log(VQ) \quad (2)$$

$\mu_j^{(i)}$ is the chemical potential of compound j in infinite dilution in pure compound i , and VQ is the volume quotient $V1/V2$. The VQ parameter is estimated using the liquid density/volume QSPR method, which may introduce inaccuracy, particularly when there is a significant density difference between the two phases. Further details regarding the COSMO and COSMO-RS calculations are provided in the previous section. The limitations of COSMO-RS arise from its ability to compute only equilibrium properties, such that kinetic and transport effects will not be captured⁵⁶.

Materials

Coloured and undyed PET fabrics, polycotton, nylon-6 (light green) and nylon-6/spandex were provided by Patagonia, Inc. Other fabrics, including denims, nylon-6 (red), and nylon-6,6 (brown), were sourced from Kontoor innovation, The ANDI Brand and authentic Cordura brand from ripstopbytheroll.com, respectively. All fabrics were identified via Fourier-transform infrared spectroscopy (FT-IR) data compared with the standard fabrics (Supplementary Fig. 27). Organic solvents including acetic acid (glacial, ACS reagent, ≥99.7%), 4-EG (≥98%, FCC, FG), 4-PG (≥99%, FG), GVL (BioRenewable, ≥99%, ReagentPlus), benzyl alcohol (ReagentPlus, ≥99%), cyrene (BioRenewable, DMF, and NMP Substitute), ε-caprolactone (97%), limonene (97%), levulinic acid (98%), valeric acid (natural, ≥98%, FG), guaiacol (natural, ≥99%, FG), eugenol (natural, ≥98%, FG), isoeugenol (natural, 99%, FG), 4-IPP (98%), thymol (≥98.5%), PEG 200 (for synthesis), PEG 400 (for synthesis), and diethylene glycol monoethyl ether (ReagentPlus, 99%) were purchased from Sigma Aldrich. Other organic solvents including 4-PP (>99%), ethanol (anhydrous, 200 proof) and EG (≥99%, laboratory reagent) were sourced from TCI Chemicals, KOPTEC and VWR Chemicals, respectively. All the organic solvents were used as received.

Batch reaction dye extraction

The PET and other fabrics were cut into ~2 cm² or smaller (equivalent to ~50 mg) per sample and submerged into a solvent (1 wt%) in a glass vial. The fabric solution was heated in a heating block on a hot plate at 100 °C for 16 h. The solvent treatment was also explored in different conditions. After the solvent treatment, the treated fabric was transferred to ethanol at room temperature (RT) for rinsing the remaining solvent on the fabric, and dried under vacuum overnight at 100–130 °C in a vacuum oven. For a larger scale than ~50 mg of fabric, a round-bottom glass flask and a reflux condenser were used.

Flow-through dye extraction

The flow-through reactor was built in-house⁵⁷ and modified. The red-jersey fabric (~5 g) was cut into small pieces (5 mm²) using a cutting machine from Cricut, and the pieces were packed in the middle of the reactor by placing them between glass wool and glass beads. The reactor was filled with glacial acetic acid at RT using a flow rate of 50 ml min⁻¹ through a pump with PEEK fluid path (Semba Octave BIO 100 Pump) to reach the operating pressure of 100 psig. High-pressure nitrogen was used to regulate the reactor pressure during the experiments. The solvent flow rate was adjusted to 1 ml min⁻¹. Preheating was required for 30–60 min to reach an operating temperature of 100 °C in the reactor. During preheating, the first liquid sample of solvent containing extracted dye was collected in the sampling pot. After 100 °C

was reached, the extracted dye solution was collected every 30 min for 120–150 min. For the 150 °C and 180 °C samples, a second heating step was required after the initial period at 100 °C. After the dye extraction was finished, the remaining solvent in the reactor was drained, and the pressure was released to take out the fabrics. The dye-extracted fabrics were rinsed with ethanol and dried in vacuum overnight.

Spectrophotometry

Colour and UV–Vis measurements were performed using UltraScan VIS from Hunter Lab and GENESYS 50 from Thermo Scientific. Reflectance and transmittance modes were used for colour and UV–Vis measurements, respectively.

High-temperature GPC

A Tosoh EcoSec HLC-8321 High-Temperature GPC System with an autosampler and a differential refractive index detector were used. The mobile phase used was *o*-chlorophenol (OCB) (HPLC Grade, Sigma Aldrich). Tosoh's Polystyrene-Quick Kit-M (PN 21916) was used to create the calibration curve from a series of polystyrene M_w standards. The solvent stock was set to 40 °C, while the pump oven was set to 50 °C. The columns, differential refractive index detector, injector valve and autosampler were all set to 110 °C. 6–20 mg of sample was placed in a Tosoh high-temperature 26-μm stainless-steel mesh filter, and OCB solvent was added to reach an end concentration of ~1.7 mg ml⁻¹ and heated on the autosampler for 2 h with occasional agitation. Run times for all standards and samples were 80 minutes. Eco-Sec 8321 software (Tosoh) was used for data processing. Mark Houwink correction values were applied ($K = 12.0 \times 10^{-5}$ dl g⁻¹ and $\alpha = 0.70$ for polystyrene (ref. 58); $K = 96.3 \times 10^{-5}$ dl g⁻¹ and $\alpha = 0.658$ for PET (ref. 59)).

DSC

The melting temperature and the per cent crystallinity were measured using a DSC 25 (Discovery Series, TA Instrument). The samples (5–10 mg in hermetically sealed aluminium pans) were first equilibrated at 0 °C, then heated to 300 °C and held at 300 °C for 5 min. Heating and cooling steps were performed at a ramp rate of 10 °C min⁻¹. The per cent crystallinity was calculated on the basis of the heat of fusion for 100% crystalline PET (140 J g⁻¹)^{54,55}.

TGA

Thermal degradation was tested using a TGA 5500 (Discovery Series, TA Instrument). The samples (5–10 mg) were heated from ambient temperature to 700 °C at 10 °C min⁻¹ under nitrogen.

X-ray scattering

X-ray scattering measurements were conducted using a Xeuss 2.0 instrument from Xenocs with a Cu Kα source. Small-angle X-ray scattering (SAXS) and wide-angle X-ray scattering (WAXS) data were collected simultaneously using a 1M Pilatus solid state detector and a 100K Dectris detector, respectively. X-ray scattering measurements were conducted with sample-to-detector distances of ~368 mm (WAXS) and 1,207 mm (SAXS) under high flux collimation (slit 1 at 1.5 mm × 1.5 mm, slit 2 at 0.7 mm × 0.7 mm). Dry fabrics were mounted to the transmission stage with Kapton polyimide tape. Swollen fabrics were loaded into gel sample holders between two 12.5-μm-thick polyimide windows to eliminate solvent evaporation. An empty gel sample holder was also prepared to remove the scattering contribution of the polyimide window, using the following equation:

$$I_{\text{intrinsic}}(q) = \frac{I_s(q)}{T_s} - \frac{I_{\text{empty}}(q)}{T_{\text{empty}}} \quad (3)$$

where I_s and I_{empty} are the transmitted intensities of the sample and the empty cell. T_s is the transmittance of the cell with the sample, and T_{empty} is the transmittance of the empty cell.

Per cent crystallinity was determined by fitting the amorphous halo to a double-Gaussian function and the crystalline peaks to Lorentzian functions; an example fit is shown in Supplementary Fig. 28. Dividing the integral of the crystalline signal by the total signal revealed the crystallinity by X-ray scattering. The long-period spacing was determined from the prominent peak at ~0.09 Å⁻¹ in Lorentz-corrected SAXS data (see representative SAXS data and Lorentz-corrected SAXS data in Supplementary Fig. 29). The crystalline peaks were consistent with the triclinic unit cell reported in PET, and the $d_{(100)}$ spacing was given by the sharp peak at $Q \approx 1.78 \text{ Å}^{-1}$.

FT-IR

A PerkinElmer FT-IR Spectrum 3 spectrometer equipped with a Universal ATR Sampling Accessory containing a Diamond/ZnSe crystal with one laser bounce was used. A background spectrum was run before each polymer sample. Each spectrum was run at ambient temperature with a wavenumber range of 650–4,000 cm⁻¹, a resolution of 4 cm⁻¹, and an accumulation of 16 scans. The force gauge was set at 75–80% of maximum pressure. All spectra were analysed using PerkinElmer Spectrum IR and Wiley KnowItAll software.

Membrane-based separation via OSN

Membrane permeability and dye rejection rates were evaluated using a dead-end filtration cell (Sterlitech HP4750). The cell contained an effective membrane area of 14.6 cm². The OSN performance was characterized by using a commercial organic nanofiltration membrane (BORSIG oNF-2, Sterlitech) with the as-extracted dye/acetic acid solutions (dye concentration, 2–5 wt%) as the feed at RT at 500 psi of applied pressure with inert nitrogen gas. The volume of the feed was 300 ml. A stir bar was added to the filtration cell. All membranes were pre-compacted by pure acetic acid at 500 psi.

Membrane permeability (*Permeability*) was calculated as follows:

$$\text{Permeability} = \frac{\Delta V}{A \Delta t \Delta P} \quad (4)$$

where ΔV is the volume of permeate collected during the time Δt , A is the membrane area and ΔP is the applied transmembrane pressure for the filtration experiment.

The dye rejection rate (R) was calculated as follows:

$$R = \left(1 - \frac{C_p}{C_f}\right) \times 100 \% \quad (5)$$

where C_p and C_f represent the dye concentration of the permeate and the feed solution (10 ml each), respectively. Their concentrations were determined using a total organic carbon (TOC) analyser (Shimadzu, TOC-L).

Additionally, a multi-pass membrane experiment was performed to recover acetic acid and evaluate the overall dye rejection rate. The overall dye rejection rate was defined as the overall percentage of dye removal after a complete passage of the OSN membrane during the entire duration of the batch process with 300 ml of total volume as the starting feed solution. The permeate from the previous stage was used as the feed for the next stage. The dye concentrations of the permeate at different stages were determined using the TOC analyser.

CCC-based separation

The counter-current chromatography instrument (S1000, Dynamic Extractions) had a rotor with a column consisting of a length of perfluoroalkoxy tubing (inner diameter, 4 mm) coiled on two bobbins. The column volume was 81 ml. A chiller was attached to the CCC to maintain a constant temperature in the instrument chamber of 25 °C. The inlet and outlet of the column were connected to an HPLC system via flying leads tubing. The HPLC system was controlled by Clarity software (v.8.1).

The four extracted dye mixtures were separated using CCC. The solvent system for CCC was prepared by mixing heptane (Reagent-Plus, 99%, Sigma Aldrich), cyclopentyl methyl ether ($\geq 99.9\%$, Sigma Aldrich), methanol (Certified ACS, Fisher Chemical), and water (18-ohm M laboratory deionized water, Thermo Scientific) (HCMWat) at a 3:1:3:1 volume ratio with a total volume of 800 ml. When the HCMWat solvent system reached equilibrium after mixing, the upper and lower phases were taken separately using separate funnels, and then used for CCC stationary and mobile phases, respectively. For all dye mixtures, the feed samples were prepared by dissolving the dried extracted dyes in the HCMWat solution (50/50% UP and LP; dye concentration, 2–5 wt%) and were loaded on the sample loop (4.5 ml) using a six-way switching valve. For all samples, the operation conditions were as follows: a CCC rotation speed of 1,400 rpm, a flow rate of 2 ml min^{-1} , sample injection 4.5 ml of the extracted dyes ($100\text{--}300 \text{ mg ml}^{-1}$) diluted in HCMWat lower phase, the reverse phase in head-to-tail mode (lower mobile phase), and elution extrusion mode started at 30 min by loading the upper phase solution. The effluent fractions were collected every 2 ml.

LC–MS

The CCC effluents were analysed on an Agilent 1100 LC system (Agilent Technologies) equipped with a diode array detector and a G6120A single quadrupole mass spectrometer. Each sample was injected at a volume of 5 μl on a Phenomenex Kinetex 1.7 μm EVO C18 100 column (Phenomenex, 2.1 mm \times 100 mm, PN 00D-4726-AN). The column temperature was maintained at 30 °C, and the buffers used were 0.1% formic acid in water (A) and 0.1% formic acid in acetonitrile (B). The flow rate was held constant at 0.4 ml min^{-1} , resulting in a run time of 29 min. The mass spectrometer was scanned in both positive and negative mode from 100 to 1,500 m/z with a gas temperature of 350 °C, drying gas flow at 12.0 l min^{-1} , a nebulizer pressure of 40 psig, and a VCap of 3,500 v in both positive and negative mode electrospray. The diode array detector scanned from 245 nm to 900 nm UV–Vis ranges and plotted 254 nm, 280 nm, and 360 nm wavelengths. The total ion chromatogram and diode array detector data were used to compare and tentatively identify candidates, by mass to charge ratio (m/z) and wavelength, of dyes detected in samples. Compounds that exhibited strong signals in the visible range (380–700 nm) were assumed to be dyes, and m/z values were recorded. Compounds reported here were all observed in positive mode and assumed to be $[\text{M} + \text{H}]^+$ m/z ions, although other adducts are possible.

Dyeing and redyeing of the dye-free PET fabric

The exhaust dyeing method and materials provided by Archroma, Inc. were adopted. First, a dyeing solution was prepared with a dried disperse dye (5 wt%) and a mixture of textile additives in 1 l of deionized water. The fabric subjected to dyeing (50 mg, 1 wt%) was added to the dyeing solution (5 ml) in a microwave vial and sealed with a pressure-resistant cap. The solution was heated under stirring in an oil bath at 130 °C for 1 h and then cooled down to 80 °C, and an after-clearing agent (3.5 g l^{-1}) was added to the solution. The solution was stirred at 80 °C for 20 min as the reduction clear step. The dyed fabric was rinsed with deionized water at RT and dried in vacuum at 100 °C overnight.

Inductively coupled plasma optical emission spectroscopy analysis

To measure the concentrations of elements including chromium, iron, magnesium, nickel, and titanium in the dye-extracted solution from the flow-through reactor, samples were prepared via microwave-assisted digestion using a Milestone Ultrawave Single Reaction Chamber Microwave Digester with a 15-vial rack. 0.1 g of each sample was digested in a combination of 4 ml of concentrated nitric acid (68–70%, ARISTAR, ACS, VWR Chemicals), 1 ml of fluoroboric acid (50%, laboratory, Fisher Chemical), and 1 ml of deionized water. After digestion, the samples

were diluted to 20 ml with deionized water to produce a clear solution. The solution was analysed using an Agilent 5110 inductively coupled plasma optical emission spectrometer. The following wavelengths and modes were used: 283.563 nm axial for Cr, 259.940 nm axial for Fe, 280.270 nm radial for Mg, 221.648 nm axial for Ni, and 336.122 nm axial for Ti. Calibration standards were measured using a six-point calibration curve (0.1–20 ppm) and had correlations of $R \geq 0.995$.

Reporting summary

Further information on research design is available in the Nature Portfolio Reporting Summary linked to this article.

Data availability

The data that support the findings presented in this paper are available in the Supplementary Information.

References

1. Zhang, L., Leung, M. Y., Boriskina, S. & Tao, X. Advancing life cycle sustainability of textiles through technological innovations. *Nat. Sustain.* **6**, 243–253 (2022).
2. Amicarelli, V., Bux, C., Spinelli, M. P. & Lagioia, G. Life cycle assessment to tackle the take-make-waste paradigm in the textiles production. *Waste Manage.* **151**, 10–27 (2022).
3. Mu, B. et al. Rapid fiber-to-fiber recycling of poly(ethylene terephthalate) and its dye from waste textiles without damaging their chemical structures. *Resour. Conserv. Recycl.* **197**, 107102 (2023).
4. TERASIL W/W-EL/WW Disperse Dyes Technical Datasheet (Huntsman, 2011).
5. Preferred Fiber and Materials Market Report (Textile Exchange, 2022).
6. Tanaka, S. et al. Depolymerization of polyester fibers with dimethyl carbonate-aided methanolysis. *ACS Mater. Au* **4**, 335–345 (2024).
7. Andini, E., Bhalode, P., Gantert, E., Sadula, S. & Vlachos, D. G. Chemical recycling of mixed textile waste. *Sci. Adv.* **10**, eado6827 (2024).
8. Kouji Mukai, M. N. Method for recovering useful components from dyed polyester fiber. US patent 7,959,807 B2 (2011).
9. Liu, P.-C., Cheng, H.-L. & Wang, C.-T. Method for decolorization of a dyed polyester fiber. US patent 2015/0059103 A1 (2015).
10. Liao, T.-C., Chuang, J.-J., Huang, Z.-M. & Huang, Z.-J. Method for decolorization of dyed polyester fiber. US patent 10,876,240 B2 (2020).
11. Mu, B. & Yang, Y. Complete separation of colorants from polymeric materials for cost-effective recycling of waste textiles. *Chem. Eng. J.* **427**, 131570 (2022).
12. Chen, Z. et al. Closed-loop utilization of polyester in the textile industry. *Green Chem.* **25**, 4429–4437 (2023).
13. West, J. C. Extraction and analysis of disperse dyes on polyester textiles. *J. Chromatogr.* **208**, 47–54 (1981).
14. Beattie, I. B., Dudley, R. J. & Smalldon, K. W. The extraction and classification of dyes on single nylon, polyacrylonitrile and polyester fibres. *J. Soc. Dyers Colour.* **95**, 295–302 (2008).
15. Amenaghawon, A. N., Anyalewechi, C. L., Kusuma, H. S. & Mahfud, M. in *Green Sustainable Process for Chemical and Environmental Engineering Science* (eds Inamuddin & Altalhi, T.) 329–346 (Elsevier, 2020).
16. Mu, B. et al. Complete recycling of polymers and dyes from polyester/cotton blended textiles via cost-effective and destruction-minimized dissolution, swelling, precipitation, and separation. *Resour. Conserv. Recycl.* **199**, 107275 (2023).
17. Thiounn, T. & Smith, R. C. Advances and approaches for chemical recycling of plastic waste. *J. Polym. Sci.* **58**, 1347–1364 (2020).
18. Luque, F. J. A. R. *Bio-Based Solvents* (John Wiley & Sons, 2017).

19. Marszatek, J. & Żyłta, R. Recovery of water from textile dyeing using membrane filtration processes. *Processes* **9**, 1833 (2021).
20. Abdelhamid, A. E., Elsayed, A. E., Naguib, M. & Ali, E. A. Effective dye removal by acrylic-based membrane constructed from textile fibers waste. *Fibers Polym.* **24**, 2391–2399 (2023).
21. Berthod, A. & Faure, K. in *Analytical Separation Science* (eds Anderson, J. et al.) Vol. 4, 1177–1206 (Wiley, 2015).
22. Bowman, Y. I. A. R. L. Countercurrent chromatography: liquid–liquid partition chromatography without solid support. *Science* **167**, 281–283 (1970).
23. Okaa, H. et al. Separation of lac dye components by high-speed counter-current chromatography. *J. Chromatogr. A* **813**, 71–77 (1998).
24. Oka, H. et al. Purification of quinoline yellow components using high-speed counter-current chromatography by stepwise increasing the flow-rate of the mobile phase. *J. Chromatogr.* **989**, 249–255 (2003).
25. Gürses, A., Açıkyıldız, M., Güneş, K. & Sadi Gürses, M. *Dyes and Pigments* (Springer, 2016).
26. Klamt, A., Jonas, V., Bürger, T. & Lohrenz, J. C. W. Refinement and parametrization of COSMO-RS. *J. Phys. Chem. A* **102**, 5074–5085 (1998).
27. Eckert, F. & Klamt, A. Fast solvent screening via quantum chemistry: COSMO-RS approach. *AIChE J.* **48**, 369–385 (2004).
28. Klamt, A. Conductor-like screening model for real solvents: a new approach to the quantitative calculation of solvation phenomena. *J. Phys. Chem.* **99**, 2224–2235 (1995).
29. Frisch, M. et al. Gaussian 16 Revision C. 01. 2016 (Gaussian Inc., 2016).
30. BIOVIA COSMOtherm v.22.0. 0 (Dassault Systèmes, 2022).
31. Van Krevelen, D. W. & Nijenhuis, K. T. *Properties of Polymers: Their Correlation with Chemical Structure; Their Numerical Estimation and Prediction from Additive Group Contributions* (Elsevier, 2009).
32. Wang, A. et al. A simple and convenient strategy for the oxidation of C(sp³)-H bonds based on γ-valerolactone. *Green Chem.* **26**, 353–361 (2024).
33. de Gonzalo, G., Alcantara, A. R. & Dominguez de Maria, P. Cyclopentyl methyl ether (CPME): a versatile eco-friendly solvent for applications in biotechnology and biorefineries. *ChemSusChem* **12**, 2083–2097 (2019).
34. Mukushi, T. et al. Multi-stage flash distillation plant. US Patent 3966562A (1976).
35. Cavin, V. C. & Acker, W. H. Process and apparatus for flash distillation. US Patent 2,805,981 (1957).
36. Parikh, N. H. *Study on Growth of Exports of Dye and Dye Intermediaries in Past Few Years* (Institute of Management, NU, 2021).
37. Enking, J. et al. Recycling processes of polyester-containing textile waste—a review. *Resour. Conserv. Recycl.* **219**, 108256 (2025).
38. Brooks, B. R. et al. CHARMM: the biomolecular simulation program. *J. Comput. Chem.* **30**, 1545–1614 (2009).
39. Phillips, J. C. et al. Scalable molecular dynamics on CPU and GPU architectures with NAMD. *J. Chem. Phys.* **153**, 044130 (2020).
40. Guvench, O. et al. Additive empirical force field for hexopyranose monosaccharides. *J. Comput. Chem.* **29**, 2543–2564 (2008).
41. Guvench, O. et al. CHARMM additive all-atom force field for glycosidic linkages between hexopyranoses. *J. Chem. Theory Comput.* **5**, 2353–2370 (2009).
42. Vanommeslaeghe, K. et al. CHARMM general force field: a force field for drug-like molecules compatible with the CHARMM all-atom additive biological force fields. *J. Comput. Chem.* **31**, 671–690 (2010).
43. Yu, W., He, X., Vanommeslaeghe, K. & MacKerell, A. D. Jr. Extension of the CHARMM general force field to sulfonyl-containing compounds and its utility in biomolecular simulations. *J. Comput. Chem.* **33**, 2451–2468 (2012).
44. Jorgensen, W. L. et al. Comparison of simple potential functions for simulating liquid water. *J. Chem. Phys.* **79**, 926–935 (1983).
45. Durell, S. R., Brooks, B. R. & Ben-Naim, A. Solvent-induced forces between two hydrophilic groups. *J. Chem. Phys.* **98**, 2198–2202 (1994).
46. Daubeny, R. D. P., Bunn, C. W., Brown, C. J. & Bragg, W. L. The crystal structure of polyethylene terephthalate. *Proc. R. Soc. Lond. A* **226**, 531–542 (1954).
47. Frenkel, D. & Smit, B. *Understanding Molecular Simulation: From Algorithms to Applications* (Elsevier, 2023).
48. Martyna, G. J., Tobias, D. J. & Klein, M. L. Constant pressure molecular dynamics algorithms. *J. Chem. Phys.* **101**, 4177–4189 (1994).
49. Feller, S. E., Zhang, Y., Pastor, R. W. & Brooks, B. R. Constant pressure molecular dynamics simulation: the Langevin piston method. *J. Chem. Phys.* **103**, 4613–4621 (1995).
50. Essmann, U. et al. A smooth particle mesh Ewald method. *J. Chem. Phys.* **103**, 8577–8593 (1995).
51. Kräutler, V., van Gunsteren, W. F. & Hünenberger, P. H. A fast SHAKE algorithm to solve distance constraint equations for small molecules in molecular dynamics simulations. *J. Comput. Chem.* **22**, 501–508 (2001).
52. Zhou, P., Sanchez-Rivera, K. L., Huber, G. W. & Van Lehn, R. C. Computational approach for rapidly predicting temperature-dependent polymer solubilities using molecular-scale models. *ChemSusChem* **14**, 4307–4316 (2021).
53. Zhou, P. et al. Large-scale computational polymer solubility predictions and applications to dissolution-based plastic recycling. *Green Chem.* **25**, 4402–4414 (2023).
54. Blaine, R. L. *Polymer Heats of Fusion TN048* (TA Instruments).
55. Wunderlich, B. *Thermal Analysis* 417–431 (Academic Press, 1990).
56. Klamt, A., Eckert, F. & Arlt, W. COSMO-RS: an alternative to simulation for calculating thermodynamic properties of liquid mixtures. *Annu. Rev. Chem. Biomol. Eng.* **1**, 101–122 (2010).
57. Brandner, D. G. et al. Flow-through solvolysis enables production of native-like lignin from biomass. *Green Chem.* **23**, 5437–5441 (2021).
58. Evans, J. M. Gel permeation chromatography: a guide to data interpretation. *Polym. Eng. Sci.* **13**, 401–408 (2004).
59. *Mark-Houwink Parameters for Polymers* (American Polymer Standards Corporation, 2022).

Acknowledgements

This work was authored in part by the National Renewable Energy Laboratory, operated by Alliance for Sustainable Energy, LLC, for the US Department of Energy under Contract No. DE-AC36-08GO28308. Funding was provided by Patagonia, Inc., through a Cooperative Research and Development Agreement and the US Department of Energy, Basic Energy Science (DOE BES DE-SC0022238) and the Office of Energy Efficiency and Renewable Energy, Advanced Materials and Manufacturing Office and Bioenergy Technologies Office. This work was performed as part of the Bio-Optimized Technologies to keep Thermoplastics out of Landfills and the Environment (BOTTLE) Consortium. The views expressed in the article do not necessarily represent the views of the US Department of Energy or the US Government. The US Government retains a non-exclusive, paid-up, irrevocable, worldwide licence to publish or reproduce the published form of this work, or allow others to do so, for US Government purposes. We thank Patagonia, Inc., for supplying textile substrates; L. Stanley for the FT-IR measurements; and B. Donohoe for analysing the optical micrographs.

Author contributions

M.L. performed dye extraction, dyeing, redyeing processes and colour measurements. A.P.-U. participated in dye extraction using a flow-through reactor. Y.L. and H.C. carried out dye separation work

using CCC. Y.L. performed OSN. A.A.C. and W.E.M. conducted the LC–MS analysis. S.Y.M. and B.C.K. performed the MD simulations and COSMO-RS calculations. J.M. and C.L. analysed PET samples using DSC and TGA. J.M. performed the high-temperature GPC analysis. E.J.F. and K.I.W. conducted the X-ray scattering experiments. J.S.D. contributed to creating the schemes in the manuscript and Supplementary Information. M.L., Y.L., A.A.C., A.P.-U., H.C. and C.W.L. contributed to designing the experimental plans. N.B. and R.D.A. contributed to discussions on the experimental results. G.T.B. and K.M.K. designed and supervised the project. M.L., Y.L., H.C., S.Y.M., B.C.K. and K.M.K. wrote the original manuscript. All authors reviewed and commented on the manuscript.

Competing interests

M.L., Y.L., A.A.C., H.C., C.W.L., R.D.A., G.T.B. and K.M.K. are authors of a patent application on methods and systems for dye removal. The other authors declare no competing interests.

Additional information

Supplementary information The online version contains supplementary material available at <https://doi.org/10.1038/s41893-025-01686-7>.

Correspondence and requests for materials should be addressed to Gregg T. Beckham or Katrina M. Knauer.

Peer review information *Nature Sustainability* thanks Zhiping Mao and the other, anonymous, reviewer(s) for their contribution to the peer review of this work.

Reprints and permissions information is available at www.nature.com/reprints.

Publisher's note Springer Nature remains neutral with regard to jurisdictional claims in published maps and institutional affiliations.

Springer Nature or its licensor (e.g. a society or other partner) holds exclusive rights to this article under a publishing agreement with the author(s) or other rightsholder(s); author self-archiving of the accepted manuscript version of this article is solely governed by the terms of such publishing agreement and applicable law.

© The Author(s), under exclusive licence to Springer Nature Limited 2025

Reporting Summary

Nature Portfolio wishes to improve the reproducibility of the work that we publish. This form provides structure for consistency and transparency in reporting. For further information on Nature Portfolio policies, see our [Editorial Policies](#) and the [Editorial Policy Checklist](#).

Statistics

For all statistical analyses, confirm that the following items are present in the figure legend, table legend, main text, or Methods section.

n/a Confirmed

- The exact sample size (n) for each experimental group/condition, given as a discrete number and unit of measurement
- A statement on whether measurements were taken from distinct samples or whether the same sample was measured repeatedly
- The statistical test(s) used AND whether they are one- or two-sided
Only common tests should be described solely by name; describe more complex techniques in the Methods section.
- A description of all covariates tested
- A description of any assumptions or corrections, such as tests of normality and adjustment for multiple comparisons
- A full description of the statistical parameters including central tendency (e.g. means) or other basic estimates (e.g. regression coefficient) AND variation (e.g. standard deviation) or associated estimates of uncertainty (e.g. confidence intervals)
- For null hypothesis testing, the test statistic (e.g. F , t , r) with confidence intervals, effect sizes, degrees of freedom and P value noted
Give P values as exact values whenever suitable.
- For Bayesian analysis, information on the choice of priors and Markov chain Monte Carlo settings
- For hierarchical and complex designs, identification of the appropriate level for tests and full reporting of outcomes
- Estimates of effect sizes (e.g. Cohen's d , Pearson's r), indicating how they were calculated

Our web collection on [statistics for biologists](#) contains articles on many of the points above.

Software and code

Policy information about [availability of computer code](#)

Data collection Molecular dynamics simulations were performed in CHARMM version 4438 and subsequent minimization and dynamics were performed with NAMD 2.13.

Data analysis All COSMO data was analyzed in COSMOtherm.

For manuscripts utilizing custom algorithms or software that are central to the research but not yet described in published literature, software must be made available to editors and reviewers. We strongly encourage code deposition in a community repository (e.g. GitHub). See the Nature Portfolio [guidelines for submitting code & software](#) for further information.

Data

Policy information about [availability of data](#)

All manuscripts must include a [data availability statement](#). This statement should provide the following information, where applicable:

- Accession codes, unique identifiers, or web links for publicly available datasets
- A description of any restrictions on data availability
- For clinical datasets or third party data, please ensure that the statement adheres to our [policy](#)

The data that supports the findings presented in this paper are available in the Supplementary Information.

Research involving human participants, their data, or biological material

Policy information about studies with [human participants or human data](#). See also policy information about [sex, gender \(identity/presentation\), and sexual orientation](#) and [race, ethnicity and racism](#).

Reporting on sex and gender

Use the terms sex (biological attribute) and gender (shaped by social and cultural circumstances) carefully in order to avoid confusing both terms. Indicate if findings apply to only one sex or gender; describe whether sex and gender were considered in study design; whether sex and/or gender was determined based on self-reporting or assigned and methods used.
Provide in the source data disaggregated sex and gender data, where this information has been collected, and if consent has been obtained for sharing of individual-level data; provide overall numbers in this Reporting Summary. Please state if this information has not been collected.

Report sex- and gender-based analyses where performed, justify reasons for lack of sex- and gender-based analysis.

Reporting on race, ethnicity, or other socially relevant groupings

Please specify the socially constructed or socially relevant categorization variable(s) used in your manuscript and explain why they were used. Please note that such variables should not be used as proxies for other socially constructed/relevant variables (for example, race or ethnicity should not be used as a proxy for socioeconomic status).

Provide clear definitions of the relevant terms used, how they were provided (by the participants/respondents, the researchers, or third parties), and the method(s) used to classify people into the different categories (e.g. self-report, census or administrative data, social media data, etc.)

Please provide details about how you controlled for confounding variables in your analyses.

Population characteristics

Describe the covariate-relevant population characteristics of the human research participants (e.g. age, genotypic information, past and current diagnosis and treatment categories). If you filled out the behavioural & social sciences study design questions and have nothing to add here, write "See above."

Recruitment

Describe how participants were recruited. Outline any potential self-selection bias or other biases that may be present and how these are likely to impact results.

Ethics oversight

Identify the organization(s) that approved the study protocol.

Note that full information on the approval of the study protocol must also be provided in the manuscript.

Field-specific reporting

Please select the one below that is the best fit for your research. If you are not sure, read the appropriate sections before making your selection.

Life sciences

Behavioural & social sciences

Ecological, evolutionary & environmental sciences

For a reference copy of the document with all sections, see nature.com/documents/nr-reporting-summary-flat.pdf

Life sciences study design

All studies must disclose on these points even when the disclosure is negative.

Sample size

NA

Data exclusions

NA

Replication

NA

Randomization

NA

Blinding

NA

Reporting for specific materials, systems and methods

We require information from authors about some types of materials, experimental systems and methods used in many studies. Here, indicate whether each material, system or method listed is relevant to your study. If you are not sure if a list item applies to your research, read the appropriate section before selecting a response.

Materials & experimental systems

n/a	Involved in the study
<input type="checkbox"/>	Antibodies
<input type="checkbox"/>	Eukaryotic cell lines
<input type="checkbox"/>	Palaeontology and archaeology
<input type="checkbox"/>	Animals and other organisms
<input type="checkbox"/>	Clinical data
<input type="checkbox"/>	Dual use research of concern
<input type="checkbox"/>	Plants

Methods

n/a	Involved in the study
<input type="checkbox"/>	ChIP-seq
<input type="checkbox"/>	Flow cytometry
<input type="checkbox"/>	MRI-based neuroimaging

Antibodies

Antibodies used

Describe all antibodies used in the study; as applicable, provide supplier name, catalog number, clone name, and lot number.

Validation

Describe the validation of each primary antibody for the species and application, noting any validation statements on the manufacturer's website, relevant citations, antibody profiles in online databases, or data provided in the manuscript.

Eukaryotic cell lines

Policy information about [cell lines](#) and [Sex and Gender in Research](#)

Cell line source(s)

State the source of each cell line used and the sex of all primary cell lines and cells derived from human participants or vertebrate models.

Authentication

Describe the authentication procedures for each cell line used OR declare that none of the cell lines used were authenticated.

Mycoplasma contamination

Confirm that all cell lines tested negative for mycoplasma contamination OR describe the results of the testing for mycoplasma contamination OR declare that the cell lines were not tested for mycoplasma contamination.

Commonly misidentified lines (See [ICLAC](#) register)

Name any commonly misidentified cell lines used in the study and provide a rationale for their use.

Palaeontology and Archaeology

Specimen provenance

Provide provenance information for specimens and describe permits that were obtained for the work (including the name of the issuing authority, the date of issue, and any identifying information). Permits should encompass collection and, where applicable, export.

Specimen deposition

Indicate where the specimens have been deposited to permit free access by other researchers.

Dating methods

If new dates are provided, describe how they were obtained (e.g. collection, storage, sample pretreatment and measurement), where they were obtained (i.e. lab name), the calibration program and the protocol for quality assurance OR state that no new dates are provided.

Tick this box to confirm that the raw and calibrated dates are available in the paper or in Supplementary Information.

Ethics oversight

Identify the organization(s) that approved or provided guidance on the study protocol, OR state that no ethical approval or guidance was required and explain why not.

Note that full information on the approval of the study protocol must also be provided in the manuscript.

Animals and other research organisms

Policy information about [studies involving animals](#); [ARRIVE guidelines](#) recommended for reporting animal research, and [Sex and Gender in Research](#)

Laboratory animals

For laboratory animals, report species, strain and age OR state that the study did not involve laboratory animals.

Wild animals

Provide details on animals observed in or captured in the field; report species and age where possible. Describe how animals were caught and transported and what happened to captive animals after the study (if killed, explain why and describe method; if released, say where and when) OR state that the study did not involve wild animals.

Reporting on sex

Indicate if findings apply to only one sex; describe whether sex was considered in study design, methods used for assigning sex. Provide data disaggregated for sex where this information has been collected in the source data as appropriate; provide overall

numbers in this Reporting Summary. Please state if this information has not been collected. Report sex-based analyses where performed, justify reasons for lack of sex-based analysis.

Field-collected samples

For laboratory work with field-collected samples, describe all relevant parameters such as housing, maintenance, temperature, photoperiod and end-of-experiment protocol OR state that the study did not involve samples collected from the field.

Ethics oversight

Identify the organization(s) that approved or provided guidance on the study protocol, OR state that no ethical approval or guidance was required and explain why not.

Note that full information on the approval of the study protocol must also be provided in the manuscript.

Clinical data

Policy information about [clinical studies](#)

All manuscripts should comply with the ICMJE [guidelines for publication of clinical research](#) and a completed [CONSORT checklist](#) must be included with all submissions.

Clinical trial registration

Provide the trial registration number from ClinicalTrials.gov or an equivalent agency.

Study protocol

Note where the full trial protocol can be accessed OR if not available, explain why.

Data collection

Describe the settings and locales of data collection, noting the time periods of recruitment and data collection.

Outcomes

Describe how you pre-defined primary and secondary outcome measures and how you assessed these measures.

Dual use research of concern

Policy information about [dual use research of concern](#)

Hazards

Could the accidental, deliberate or reckless misuse of agents or technologies generated in the work, or the application of information presented in the manuscript, pose a threat to:

No	Yes
<input checked="" type="checkbox"/>	<input type="checkbox"/> Public health
<input checked="" type="checkbox"/>	<input type="checkbox"/> National security
<input checked="" type="checkbox"/>	<input type="checkbox"/> Crops and/or livestock
<input checked="" type="checkbox"/>	<input type="checkbox"/> Ecosystems
<input checked="" type="checkbox"/>	<input type="checkbox"/> Any other significant area

Experiments of concern

Does the work involve any of these experiments of concern:

No	Yes
<input checked="" type="checkbox"/>	<input type="checkbox"/> Demonstrate how to render a vaccine ineffective
<input type="checkbox"/>	<input type="checkbox"/> Confer resistance to therapeutically useful antibiotics or antiviral agents
<input checked="" type="checkbox"/>	<input type="checkbox"/> Enhance the virulence of a pathogen or render a nonpathogen virulent
<input checked="" type="checkbox"/>	<input type="checkbox"/> Increase transmissibility of a pathogen
<input checked="" type="checkbox"/>	<input type="checkbox"/> Alter the host range of a pathogen
<input checked="" type="checkbox"/>	<input type="checkbox"/> Enable evasion of diagnostic/detection modalities
<input checked="" type="checkbox"/>	<input type="checkbox"/> Enable the weaponization of a biological agent or toxin
<input checked="" type="checkbox"/>	<input type="checkbox"/> Any other potentially harmful combination of experiments and agents

Plants

Seed stocks	<i>Report on the source of all seed stocks or other plant material used. If applicable, state the seed stock centre and catalogue number. If plant specimens were collected from the field, describe the collection location, date and sampling procedures.</i>
Novel plant genotypes	<i>Describe the methods by which all novel plant genotypes were produced. This includes those generated by transgenic approaches, gene editing, chemical/radiation-based mutagenesis and hybridization. For transgenic lines, describe the transformation method, the number of independent lines analyzed and the generation upon which experiments were performed. For gene-edited lines, describe the editor used, the endogenous sequence targeted for editing, the targeting guide RNA sequence (if applicable) and how the editor was applied.</i>
Authentication	<i>Describe any authentication procedures for each seed stock used or novel genotype generated. Describe any experiments used to assess the effect of a mutation and, where applicable, how potential secondary effects (e.g. second site T-DNA insertions, mosaicism, off-target gene editing) were examined.</i>

ChIP-seq

Data deposition

- Confirm that both raw and final processed data have been deposited in a public database such as [GEO](#).
- Confirm that you have deposited or provided access to graph files (e.g. BED files) for the called peaks.

Data access links

May remain private before publication.

For "Initial submission" or "Revised version" documents, provide reviewer access links. For your "Final submission" document, provide a link to the deposited data.

Files in database submission

Provide a list of all files available in the database submission.

Genome browser session (e.g. [UCSC](#))

Provide a link to an anonymized genome browser session for "Initial submission" and "Revised version" documents only, to enable peer review. Write "no longer applicable" for "Final submission" documents.

Methodology

Replicates	<i>Describe the experimental replicates, specifying number, type and replicate agreement.</i>
Sequencing depth	<i>Describe the sequencing depth for each experiment, providing the total number of reads, uniquely mapped reads, length of reads and whether they were paired- or single-end.</i>
Antibodies	<i>Describe the antibodies used for the ChIP-seq experiments; as applicable, provide supplier name, catalog number, clone name, and lot number.</i>
Peak calling parameters	<i>Specify the command line program and parameters used for read mapping and peak calling, including the ChIP, control and index files used.</i>
Data quality	<i>Describe the methods used to ensure data quality in full detail, including how many peaks are at FDR 5% and above 5-fold enrichment.</i>
Software	<i>Describe the software used to collect and analyze the ChIP-seq data. For custom code that has been deposited into a community repository, provide accession details.</i>

Flow Cytometry

Plots

Confirm that:

- The axis labels state the marker and fluorochrome used (e.g. CD4-FITC).
- The axis scales are clearly visible. Include numbers along axes only for bottom left plot of group (a 'group' is an analysis of identical markers).
- All plots are contour plots with outliers or pseudocolor plots.
- A numerical value for number of cells or percentage (with statistics) is provided.

Methodology

Sample preparation	<i>Describe the sample preparation, detailing the biological source of the cells and any tissue processing steps used.</i>
Instrument	<i>Identify the instrument used for data collection, specifying make and model number.</i>
Software	<i>Describe the software used to collect and analyze the flow cytometry data. For custom code that has been deposited into a community repository, provide accession details.</i>

Cell population abundance

Describe the abundance of the relevant cell populations within post-sort fractions, providing details on the purity of the samples and how it was determined.

Gating strategy

Describe the gating strategy used for all relevant experiments, specifying the preliminary FSC/SSC gates of the starting cell population, indicating where boundaries between "positive" and "negative" staining cell populations are defined.

Tick this box to confirm that a figure exemplifying the gating strategy is provided in the Supplementary Information.

Magnetic resonance imaging

Experimental design

Design type

Indicate task or resting state; event-related or block design.

Design specifications

Specify the number of blocks, trials or experimental units per session and/or subject, and specify the length of each trial or block (if trials are blocked) and interval between trials.

Behavioral performance measures

State number and/or type of variables recorded (e.g. correct button press, response time) and what statistics were used to establish that the subjects were performing the task as expected (e.g. mean, range, and/or standard deviation across subjects).

Acquisition

Imaging type(s)

Specify: functional, structural, diffusion, perfusion.

Field strength

Specify in Tesla

Sequence & imaging parameters

Specify the pulse sequence type (gradient echo, spin echo, etc.), imaging type (EPI, spiral, etc.), field of view, matrix size, slice thickness, orientation and TE/TR/flip angle.

Area of acquisition

State whether a whole brain scan was used OR define the area of acquisition, describing how the region was determined.

Diffusion MRI

Used

Not used

Preprocessing

Preprocessing software

Provide detail on software version and revision number and on specific parameters (model/functions, brain extraction, segmentation, smoothing kernel size, etc.).

Normalization

If data were normalized/standardized, describe the approach(es): specify linear or non-linear and define image types used for transformation OR indicate that data were not normalized and explain rationale for lack of normalization.

Normalization template

Describe the template used for normalization/transformation, specifying subject space or group standardized space (e.g. original Talairach, MNI305, ICBM152) OR indicate that the data were not normalized.

Noise and artifact removal

Describe your procedure(s) for artifact and structured noise removal, specifying motion parameters, tissue signals and physiological signals (heart rate, respiration).

Volume censoring

Define your software and/or method and criteria for volume censoring, and state the extent of such censoring.

Statistical modeling & inference

Model type and settings

Specify type (mass univariate, multivariate, RSA, predictive, etc.) and describe essential details of the model at the first and second levels (e.g. fixed, random or mixed effects; drift or auto-correlation).

Effect(s) tested

Define precise effect in terms of the task or stimulus conditions instead of psychological concepts and indicate whether ANOVA or factorial designs were used.

Specify type of analysis: Whole brain ROI-based Both

Specify voxel-wise or cluster-wise and report all relevant parameters for cluster-wise methods.

Statistic type for inference

(See [Eklund et al. 2016](#))

Correction

Describe the type of correction and how it is obtained for multiple comparisons (e.g. FWE, FDR, permutation or Monte Carlo).

Models & analysis

n/a Involved in the study

- Functional and/or effective connectivity
- Graph analysis
- Multivariate modeling or predictive analysis

Functional and/or effective connectivity

Report the measures of dependence used and the model details (e.g. Pearson correlation, partial correlation, mutual information).

Graph analysis

Report the dependent variable and connectivity measure, specifying weighted graph or binarized graph, subject- or group-level, and the global and/or node summaries used (e.g. clustering coefficient, efficiency, etc.).

Multivariate modeling and predictive analysis

Specify independent variables, features extraction and dimension reduction, model, training and evaluation metrics.